J Mater Sci (2016) 51:2841–2849
DOI 10.1007/s10853-015-9592-x

Tunable emission, energy transfer, and thermal stability of Ce^{3+}-doped and Ce^{3+}/Tb^{3+} Co-doped $Ca_9Sr(PO_4)_6Cl_2$ phosphors

Lijuan Feng[1] · Yue Tian[1] · Lei Wang[1] · Cai'e Cui[1] · Qiufeng Shi[1] · Ping Huang[1]

Received: 1 September 2015 / Accepted: 13 November 2015 / Published online: 19 November 2015

Abstract Ce^{3+}-doped and Ce^{3+}/Tb^{3+} co-doped $Ca_9Sr(PO_4)_6Cl_2$ phosphors were synthesized successfully via a traditional high-temperature solid-state reaction. The crystal structure, photoluminescent properties including temperature-dependent luminescence, and energy transfer of the as-prepared phosphors were investigated. The as-prepared $Ca_9Sr(PO_4)_6Cl_2:Ce^{3+}$ phosphors exhibit a broad excitation band ranging from 220 to 385 nm and blue light-emitting band centered at 431 nm, which originate from the 4*f*–5*d* transitions of Ce^{3+} ion. The luminescent intensities of Tb^{3+} ions were dramatically enhanced by the introduction of Ce^{3+} in the $Ca_9Sr(PO_4)_6Cl_2:Tb^{3+}$ phosphors because of the efficient energy transfer from Ce^{3+} to Tb^{3+} ions, generating tunable blue-green emission colors. The mechanism of energy transfer between Ce^{3+} and Tb^{3+} ions was demonstrated to be an electric dipole–quadrupole interaction. Moreover, the energy transfer efficiency was evaluated up to 75 % based on the analysis of the emission spectra. The temperature-dependent photoluminescence indicates that the as-prepared Ce^{3+}/Tb^{3+} co-doped $Ca_9Sr(PO_4)_6Cl_2$ phosphors have excellent thermal stability. Our results suggest that the Ce^{3+}-doped and Ce^{3+}/Tb^{3+} co-doped $Ca_9Sr(PO_4)_6Cl_2$ phosphors have potential application for n-UV pumped WLEDs.

✉ Yue Tian
tianyue@tyut.edu.cn

✉ Ping Huang
huangpinghuangka@163.com

[1] Key Lab of Advanced Transducers and Intelligent Control System of Ministry of Education, College of Physics and Optoelectronic Engineering, Taiyuan University of Technology, Taiyuan 030024, People's Republic of China

Introduction

White light-emitting diodes (WLEDs) are considered as an ideal candidate for the replacement of conventional lighting resource because of their remarkable advantages such as long operation lifetime, high luminous efficiency, energy saving, and eco-friendliness [1–3]. Typically, the commercial WLEDs were assembled by a combination of a blue-emitting InGaN chip and a yellow-emitting $Y_3Al_5O_{12}:Ce^{3+}$ (YAG:Ce^{3+}) phosphor. However, this type of device suffers from inevitable drawbacks including a low color rendering index (CRI < 75) and high correlated color temperature (CCT ≥ 4500 K) due to the lack of red component in the visible region [5–7]. Nowadays, in view of these problems, WLEDs fabricated by assembling ultraviolet (UV) or near-ultraviolet (n-UV) LED chips and tricolor (red, green, and blue) phosphors are expected to dominate the solid-state lighting (SSL) market in the future because the white light outputting from this type of WLEDs has controlled color temperature and exceptional color rendering index [1–4]. In addition, the performances of n-UV LEDs strongly depend on the luminescence performance of phosphors used. Therefore, the recent researches have focused on developing suitable tricolor phosphors with high luminescent efficiency and high stability for n-UV LEDs [4–6].

As we all know, Tb^{3+} ion is frequently used as an activator of green-emitting luminescent phosphors because it has a relatively simple structure of energy levels that consist of ^7F_J, $^5D_4$, and $^5D_3$ states. Usually, the $^5D_4$–$^7F_5$ transition peaking at around 541 nm leads to the predominant green

emission, which is a magnetic dipole transition with $\Delta J = 1$ [9, 34]. However, the intensities of Tb^{3+} characteristic sharp lines at 488, 541, and 582 nm are very week and the spectral widths are quite narrow due to the strictly forbidden f–f absorption transitions as well. One of the efficient strategies to conquer the difficulty is to introduce Ce^{3+} as a sensitizer to transfer excitation energy to Tb^{3+} efficiently because there is larger spectral overlapping between the emission spectrum of Ce^{3+} ion and absorption spectrum of Tb^{3+} ion. Until now, several Ce^{3+}/Tb^{3+} co-doped phosphors have been synthesized and investigated, such as $Li_6Lu(BO_3)_3:Ce^{3+}$, Tb^{3+}; $Y_4Si_2O_7N_2:Ce^{3+}$, Tb^{3+}; $Ca_6Ba(PO_4)_4O:Ce^{3+}$, Tb^{3+}; $YBO_3:Ce^{3+}$, Tb^{3+}; $KGdF_4:Ce^{3+}$, Tb^{3+}; $GdPO_4:Ce^{3+}$, Tb^{3+}, and so on [3–20].

Materials belonging to the large apatite family described by the general formula of $M_{10}(TO_4)_6X_2$ (M = alkaline; X = monovalent anion, such as OH^- Cl^-, and F^-; and TO_4^{3-} = trivalent anions, such as PO_4^{3-}, VO_4^{3-}, or AsO_4^{3-}) are widely used for n-UV LEDs owing to their many advantages including high chemical and physical stability, low cost, and excellent weather resistance [21–25]. A wide range of cationic and anionic substitutions are possible to create many modified apatite structures with improved luminescent performance [25]. Especially, $Ca_{10}(PO_4)_6Cl_2$ is a good host lattice for luminescence. Recent investigation was conducted on $Ca_{10}(PO_4)_6Cl_2:Eu^{3+}$; $Ca_{10}(PO_4)_6Cl_2:Eu^{2+}$ [21, 23]. To the best of our knowledge, there is no report on the luminescence of Ce^{3+}-doped and Ce^{3+}/Tb^{3+} co-doped $Ca_9Sr(PO_4)_6Cl_2$ phosphors yet. Herein, we prepared Ce^{3+}-doped and Ce^{3+}/Tb^{3+} co-doped $Ca_9Sr(PO_4)_6Cl_2$ phosphors via a high-temperature solid-state reaction method. The crystal structure, photoluminescent (PL) properties, color chromaticity, energy transfer, and thermal quenching of the as-prepared samples were investigated. The results show that Ce^{3+}-doped and Ce^{3+}/Tb^{3+} co-doped $Ca_9Sr(PO_4)_6Cl_2$ phosphors could be a potential blue-green tunable phosphor for n-UV pumped WLEDs.

Experimental section

Synthesis

$Ca_9Sr(PO_4)_6Cl_2:x\%Ce^{3+}$ ($1 \le x \le 7$) and $Ca_9Sr(PO_4)_6Cl_2:5\%Ce^{3+}$, $y\%Tb^{3+}$ ($1 \le y \le 7$) phosphors were prepared by a solid-state reaction from a stoichiometric mixture of $CaCO_3$, $SrCl_2$, $(NH_4)_2HPO_4$, CeO_2, and Tb_4O_7. The weighed raw chemicals were ground thoroughly in an agate mortar for 2.5 h, and then the obtained mixture was sintered in alumina crucibles at 1400 °C for 5 h under CO reducing atmosphere to produce the final sample. Finally, the prepared samples were cooled to room temperature and reground for further measurements.

Characterizations

To investigate the crystal phases of the as-prepared powder, X-ray diffractions (XRD) were performed in the range of $10 \le 2\theta \le 70^\circ$ with the step of 0.02^o using a Shimadzu-6000 X-ray generator equipped with Cu K_α radiation ($\lambda = 0.15406$ nm). Diffuse reflectance spectra were measured using a Shimadzu UV-2600 spectrophotometer using the white $BaSO_4$ powder as a reference standard. Photoluminescence emission (PL) and excitation (PLE) were recorded on an F-280 fluorescence spectrophotometer with a 150 W Xe lamp as its excitation source. A home-made temperature control system was used to measure temperature-dependent emission spectra from 298 to 573 K, in which the measuring and controlling accuracy of the temperature is about ± 0.5 °C.

Results and discussion

Phase and crystal structure

The XRD patterns of $Ca_9Sr(PO_4)_6Cl_2:5\%Ce^{3+}$; $Ca_9Sr(PO_4)_6Cl_2:5\%Tb^{3+}$; and $Ca_9Sr(PO_4)_6Cl_2:5\%Ce^{3+}$, $5\%Tb^{3+}$ samples are presented in Fig. 1. It can be found that all XRD patterns have the similar profiles, which are well consistent with that of the standard hexagonal $Ca_{10}(PO_4)_6Cl_2$ reported in ICSD card with the number of 24237 (space group P63/m, no.176). No detectable phase from impurity can be observed in all the as-prepared samples even though Sr^{2+}, Ce^{3+}, and Tb^{3+} ions were introduced into the host lattice. This suggests that all of the samples are of single phase and the Sr^{2+}, Ce^{3+}, and Tb^{3+} ions have been successfully incorporated in the $Ca_{10}(PO_4)_6Cl_2$ host lattice without changing the crystal structure. In addition,

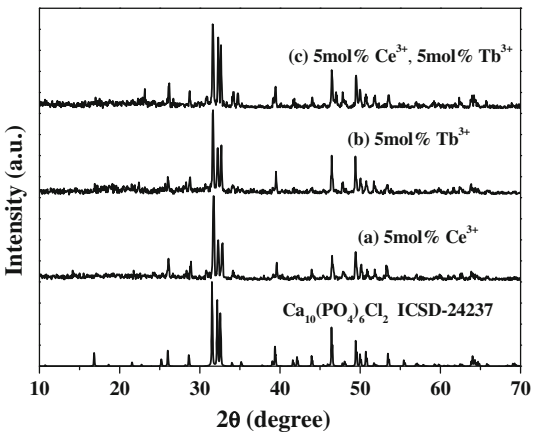

Fig. 1 Typical XRD patterns of $Ca_9Sr(PO_4)_6Cl_2:5mol\%Ce^{3+}$, $Ca_9Sr(PO_4)_6Cl_2:5mol\%Tb^{3+}$, and $Ca_9Sr(PO_4)_6Cl_2:5mol\%Ce^{3+}$, $5mol\%Tb^{3+}$ phosphors as well as the ICSD card of the standard $Ca_{10}(PO_4)_6Cl_2$ crystal

we can also see that the XRD peaks of the as-prepared samples are intense and sharp, indicating that the products are crystallized well. This is in the favor of highly efficient luminescence of rare earth ions as well.

Diffuse reflectance spectra

Figure 2 shows the diffuse reflectance spectra of $Ca_9Sr(PO_4)_6Cl_2$, $Ca_9Sr(PO_4)_6Cl_2$:5%Ce^{3+}, $Ca_9Sr(PO_4)_6Cl_2$:5%Tb^{3+}, and $Ca_9Sr(PO_4)_6Cl_2$:5%Ce^{3+}, 5%Tb^{3+} phosphors, which are good evidence of absorption in the n-UV region induced by the activator ions. For $Ca_9Sr(PO_4)_6Cl_2$ host, it can be found that a very weak absorption band ranges from 230 to 420 nm. When Ce^{3+} ions are introduced into the host, a strong and broad absorption band in the range of 230–500 nm can be observed, which is ascribed to the 4*f*–5*d* absorption of Ce^{3+} ion. For $Ca_9Sr(PO_4)_6Cl_2$:5%Tb^{3+}, the spectral profile is similar to that of the undoped host except a strong absorption peak at around 250 nm, which corresponds to the 4*f*-5*d* transition of Tb^{3+} ion [12]. However, as Ce^{3+} and Tb^{3+} ions are introduced into the host together, the intensity of absorption band of Ce^{3+} ions are improved obviously, reflecting the occurrence of an energy transfer from Ce^{3+} to Tb^{3+}. Therefore, the above results also suggest that Ce^{3+}–Tb^{3+} co-doped $Ca_9Sr(PO_4)_6Cl_2$ phosphor can be used as a blue-green tunable phosphor for n-UV LED because of an efficient absorption in the n-UV region.

Photoluminescence properties and concentration quenching of Ce^{3+} ions

Figure 3a shows the photoluminescent emission (PL) and excitation (PLE) spectra of the $Ca_9Sr(PO_4)_6Cl_2$:5%Ce^{3+} phosphor. It can be found that the PL spectrum shows a

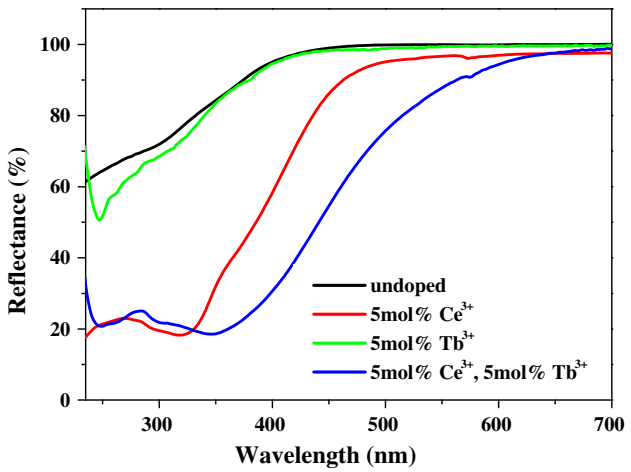

Fig. 2 The diffuse reflectance spectra of $Ca_9Sr(PO_4)_6Cl_2$:-*x* mol%Ce^{3+}, *y* mol%Tb^{3+} phosphors

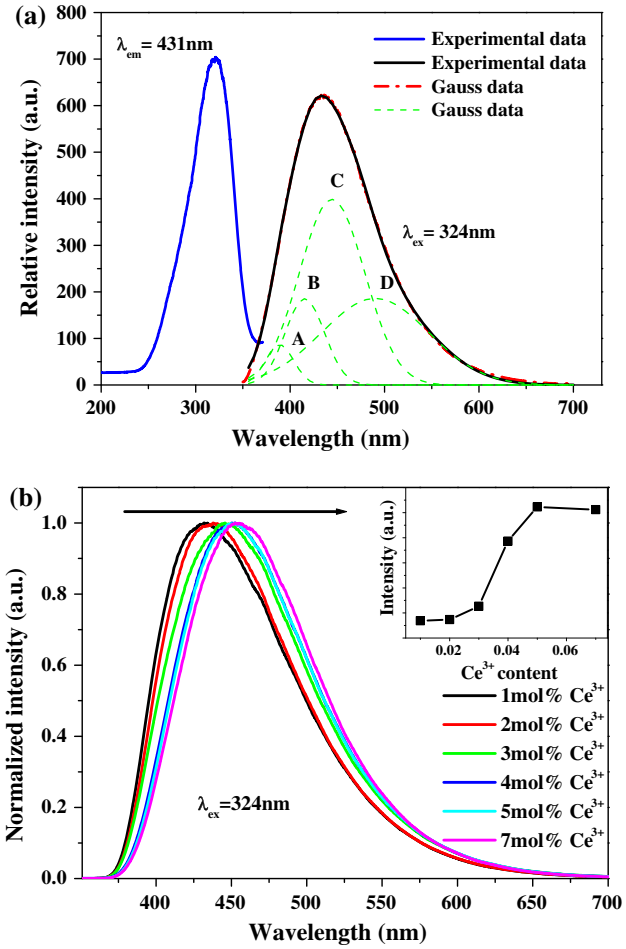

Fig. 3 **a** PL and PLE spectra of $Ca_9Sr(PO_4)_6Cl_2$:5 mol % Ce^{3+} phosphor and four Gaussian fitting emission spectra. **b** Normalized PL spectra of $Ca_9Sr(PO_4)_6Cl_2$:*x*mol%Ce^{3+} phosphors with different Ce^{3+} doping concentrations. The inset shows the dependence of luminescent intensity on the doping concentration of Ce^{3+} ions

broad nonsymmetric blue emission band extending from 360 to 700 nm with a peak centered at about 431 nm. Since there are two Ca^{2+} sites in the $Ca_9Sr(PO_4)_6Cl_2$ host and Ce^{3+} usually presents typical double emission peaks in a single definite lattice site from the lowest 5d excited state to the ^2F_J ($J = 5/2, 7/2$) spin–orbit split 4*f* ground states, the emission spectrum can be decomposed into four Gaussian components with peaks centered at 387, 418, 444, and 487 nm, which are labeled as band A, B, C, and D, respectively [9, 21, 23]. The energy gaps between A and B, and C and D are 1950 and 1989 cm^{-1}, respectively, which is in good agreement with the theoretical value of about 2000 cm^{-1} [27, 28]. From the emission spectrum, therefore, we concluded that there are two kinds of Ce^{3+} luminescent centers in the $Ca_9Sr(PO_4)_6Cl_2$ host lattice. Monitoring the emission at 431 nm, the PLE spectrum exhibits a broad band in the range from 220 to 385 nm, which is derived from the 4*f*–5*d* transition of Ce^{3+} ion. The

strongest absorption band peaked at about 324 nm, which matches well with n-UV LED chips.

In order to investigate the effect of doping concentration on the luminescent properties, a series of $Ca_9Sr(PO_4)_6Cl_2$:x%Ce^{3+} ($1 \leq x \leq 7$) phosphors were synthesized. The inset of Fig. 3b shows the dependence of emission intensity on the concentrations of Ce^{3+} ions in $Ca_9Sr(PO_4)_6Cl_2$ phosphors. It can be observed that the blue emission of the Ce^{3+} gradually increases with increasing Ce^{3+} concentration, and reaches a maximum value at $x = 5$. Continuing the doping concentration of Ce^{3+} ions, we can find that emission intensity decreases because of the concentration quenching effect. In the meantime, an obvious redshift of the emission peak wavelength is observed in Fig. 3b as the concentration of Ce^{3+} gradually increases. This phenomenon can be explained as follows. In our case, we propose that there exists an energy transfer between Ce^{3+} ions in different crystallographic sites. Thus, the intensities of four Gaussian components (Ce_A–Ce_D) originated from two kinds of Ce^{3+} increased relatively with increasing Ce^{3+} concentration, and it affected the change of emission shape and the peak position by the substitution of Ca^{2+} ions [6, 11, 28]. Furthermore, the reabsorption of the high-energy part of the emission (resonant with the low-energy part of the excitation spectra) is another possible reason for the redshift of the emission spectrum in $Ca_9Sr(PO_4)_6Cl_2$:x%Ce^{3+} ($1 \leq x \leq 7$) phosphors [29].

Usually, it is considered that concentration quenching is mainly caused by energy transfer among Ce^{3+} ions. Therefore, to further investigate the energy transfer mechanism of Ce^{3+} ions in $Ca_9Sr(PO_4)_6Cl_2$, the critical distance of energy transfer (R_c) should be evaluated first. According to the theory proposed by Blasse, the critical distance, R_c, can be expressed as follows [29, 30]:

$$R_c \approx 2\left[\frac{3V}{4\pi x_c N}\right]^{1/3}, \quad (1)$$

where V is the volume of the unit cell, x_C is the critical concentration of Ce^{3+} ions, and N is the number of host cations in the unit cell. As for $Ca_9Sr(PO_4)_6Cl_2$ host, $V = 537.64$ Å^3, $x_C = 0.05$, and $N = 10$. Therefore, the critical transfer distance R_c is calculated to be 12.71 Å. Non-radiative energy transfer may occur by exchange interaction or multi-polar interaction. The former one is dominant when the critical distance is <4 Å [30, 31]. So it can be excluded that the exchange interaction is responsible for the energy transfer between Ce^{3+} ions in $Ca_9Sr(PO_4)_6Cl_2$ host. Therefore, electric multipole should be the dominant mechanism for the energy transfer between Ce^{3+} ions in $Ca_9Sr(PO_4)_6Cl_2$:Ce^{3+} phosphors. Van Uitert has developed a phenomenological model to explain the relationship between the luminescent intensity and the concentration of luminescent center, which can be written as [32, 33]

$$\frac{I}{x} = k[1 + \beta(x)^{\theta/3}]^{-1}, \quad (2)$$

where x is the doping concentration of Ce^{3+} ions in the present case; K and β are constants for a certain system; θ represents the interaction type between luminescence center and quenching center, here $\theta = 6$, 8, or 10, indicating the exchange interaction, electric dipole–dipole (D–D), electric dipole–quadrupole (D–Q), and electric quadrupole–quadrupole (Q–Q) interactions, respectively. In order to understand the energy transfer mechanism between Ce^{3+} ions in $Ca_9Sr(PO_4)_6Cl_2$ phosphors, Eq. (2) was used to fit the experimental data in Fig. 4. It can be found that Eq. (2) fit well with the experimental data, and the θ value was deduced from the fitting process to be 6.21, which suggests that the electric dipole–dipole interaction should be responsible for the energy transfer of Ce^{3+} in $Ca_9Sr(PO_4)_6Cl_2$ phosphors.

Energy transfer from Ce^{3+} to Tb^{3+}

As for the Tb^{3+}-doped $Ca_9Sr(PO_4)_6Cl_2$ sample, its PLE and PL spectra are presented in Fig. 5b. The PL spectrum under the excitation of 379 nm displays a series of sharp-line emissions. The emission peaks at 486, 541, 590, and 618 nm are assigned to the $^5D_4$–^7F_J ($J = 6$, 5, 4, 3) characteristic transitions of Tb^{3+} ion. The green emission line at 541 nm from the $^5D_4$–$^7F_5$ transitions dominates the whole emission spectrum, which is a magnetic dipole transition with $\Delta J = 1$ [9, 34]. Therefore, the Tb^{3+}-doped $Ca_9Sr(PO_4)_6Cl_2$ sample exhibits green emission under the excitation of 379 nm. Monitoring the emission at 541 nm,

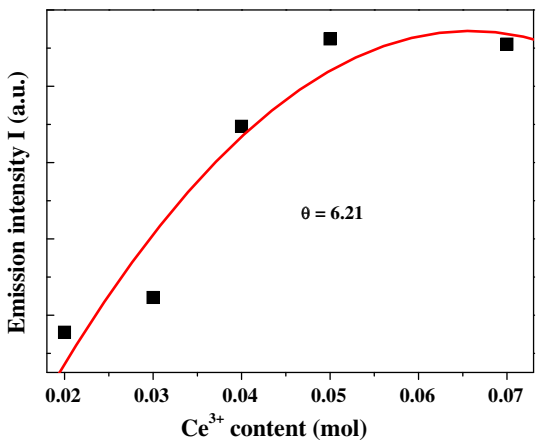

Fig. 4 Dependence of integrated emission intensity of Ce^{3+} ions on doping concentration in the $Ca_9Sr(PO_4)_6Cl_2$:Ce^{3+} phosphors. Solid curve is the fitting curve derived based on Van Uitert's model

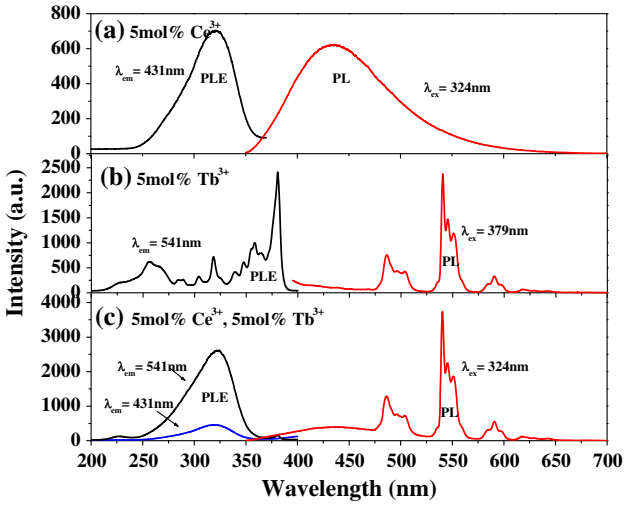

Fig. 5 PLE and PL spectra of $Ca_9Sr(PO_4)_6Cl_2$:Ce^{3+}, Tb^{3+} phosphors. **a** 5 mol% Ce^{3+}, **b** 5 mol%Tb^{3+}, and **c** 5 mol% Ce^{3+}, 5 mol% Tb^{3+}

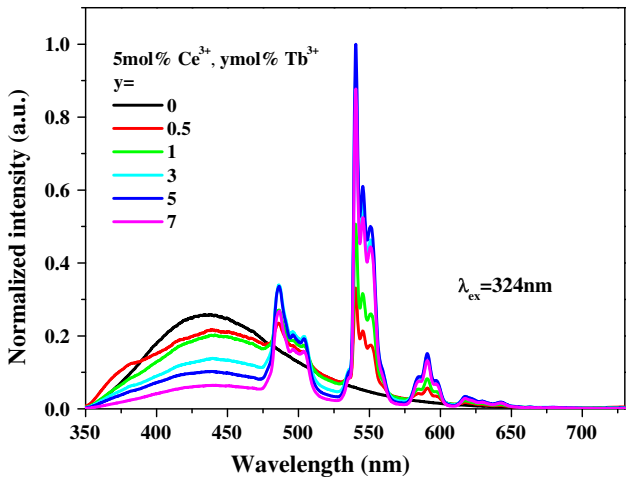

Fig. 6 PL spectra of $Ca_9Sr(PO_4)_6Cl_2$:5mol% Ce^{3+}, *y*mol%Tb^{3+} ($0 \le y \le 7$) phosphors under the excitation of 324 nm

the PLE spectrum contains a broad band and several lines. The broad band ranging from 200 to 270 nm centered at 256 nm is assigned to the 4*f*–5*d* transition of Tb^{3+} ions, while the excitation lines are attributed to the intra-4f^8 transitions of Tb^{3+} ions [2]. Comparing the PL spectra of Ce^{3+} (Fig. 5a) with the PLE spectra of Tb^{3+} (Fig. 5b), it is clearly observed that there is a spectral overlap, indicating that an effective energy transfer from the sensitizer, Ce^{3+}, to the activator, Tb^{3+}, can be expected in the $Ca_9Sr(PO_4)_6Cl_2$ host. Meanwhile, as shown in Fig. 5c, it can be found that the profile of PLE spectrum of Ce^{3+}–Tb^{3+} co-doped $Ca_9Sr(PO_4)_6Cl_2$ phosphor monitored the emission of Tb^{3+} ions at 541 nm is similar to that monitored the emission of Ce^{3+} ions at 431 nm. Moreover, when the sample was excited by 324 nm UV light, the PL spectrum shows the weaker blue emission of Ce^{3+} and the stronger green emission of Tb^{3+} comparing with that in $Ca_9Sr(PO_4)_6Cl_2$:Ce^{3+} and $Ca_9Sr(PO_4)_6Cl_2$:Tb^{3+}, which is an obvious evidence for the energy transfer from Ce^{3+} to Tb^{3+} in $Ca_9Sr(PO_4)_6Cl_2$ host [35]. The PLE spectra consist of a broad band extending from 250 to 360 nm which means that $Ca_9Sr(PO_4)_6Cl_2$:Ce^{3+},Tb^{3+} phosphor is a potential green-emitting phosphor for UV pumped WLEDs as well.

Figure 6 shows the PL spectra of the as-prepared $Ca_9Sr(PO_4)_6Cl_2$:5%molCe^{3+}, *y*%molTb^{3+} ($0 \le y \le 7$) samples under the excitation of 324 nm. It can be seen that all the emission spectra mainly consist of a broad emission band of several line peaks. This form corresponds to the 4*f*–5*d* transitions of Ce^{3+} ion and the later originates from the $^5D_4$–^7F_J ($J = 6, 5, 4, 3$) characteristic transitions of Tb^{3+} ion. Moreover, the emission intensity of the Ce^{3+} decreases monotonously with increasing the Tb^{3+} concentration when the Ce^{3+} doping concentration is fixed, which indicates an efficient energy transfer from Ce^{3+} to Tb^{3+}. From the luminescence of Tb^{3+} ions, it can be found that the emission intensity of Tb^{3+} increases gradually and reaches a maximum value when $y = 5$. As a result of concentration quenching, the emissions of Tb^{3+} decreases when the Tb^{3+} ion concentration exceeds over 5 %.

In general, the energy transfer efficiency from a sensitizer to activator, η_{ET}, can be expressed as the following equation [36]:

$$\eta_{ET} = 1 - \frac{I_s}{I_{s0}}, \tag{3}$$

where I_s is the luminescent intensity of Ce^{3+} in the presence of Tb^{3+} and I_{s0} is the luminescent intensity of Ce^{3+} in the absence of Tb^{3+}. In the $Ca_9Sr(PO_4)_6Cl_2$:Ce^{3+}, Tb^{3+} system, Ce^{3+} is the sensitizer and Tb^{3+} is the activator. Figure 7 shows the result of energy transfer efficiency from Ce^{3+} to Tb^{3+} calculated using Eq. (3). As shown in Fig. 7, the energy transfer efficiency increases with the increase of Tb^{3+} concentration. However, the increscent rate of the emission intensity gradually decreases with increasing Tb^{3+} concentration. The maximal energy transfer efficiency can reach 76 % when 7 %mol Tb^{3+} ions were doped. The above results indicate that the energy transfer from Ce^{3+} to Tb^{3+} is very efficient.

On the basis of Dexter's energy transfer formula of multi-polar interaction and Reisfeld's approximation, the following relation can be obtained [34–37]:

$$\frac{\eta_0}{\eta} \propto C^{n/3}, \tag{4}$$

where η_0 and η are the luminescent quantum efficiency of the sensitizer (Ce^{3+}) in the absence and presence of an activator (Tb^{3+}), respectively and C is the concentration of

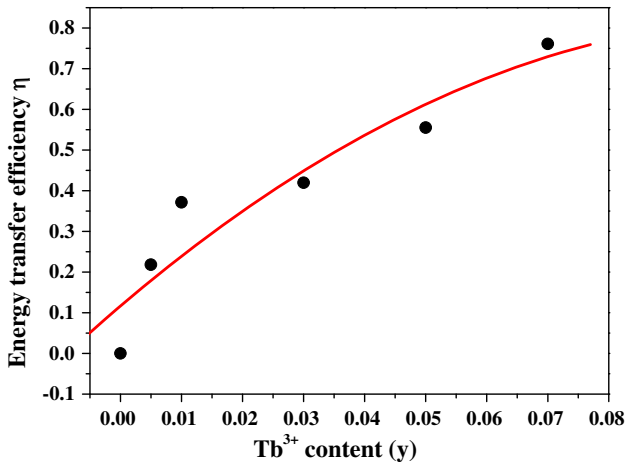

Fig. 7 Dependence of the energy transfer efficiency (η_T) from Ce^{3+} to Tb^{3+} on the Tb^{3+} doping concentration in the as-prepared $Ca_9Sr(PO_4)_6Cl_2$ phosphors

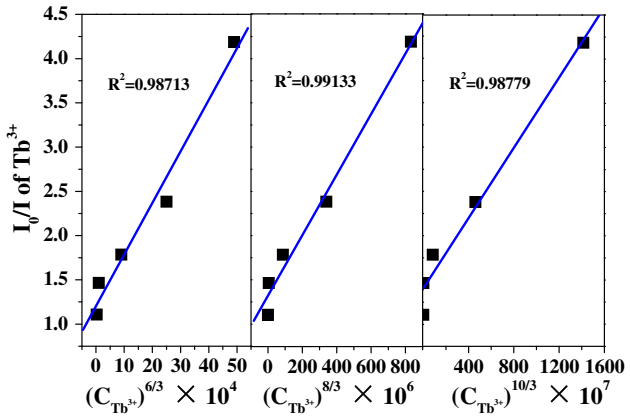

Fig. 8 Dependence of I/I_0 of Ce^{3+} ions on a $C^{6/3}$, b $C^{8/3}$, and c $C^{10/3}$

Tb^{3+} ions. The value of η_0/η was estimated by the ratio of luminescence intensities as [36–38]

$$\frac{I_0}{I_s} \propto C^{n/3}, \tag{5}$$

where I_0 and I_S are the intrinsic luminescence intensity of a sensitizer (Ce^{3+}) in the absence and presence of an activator (Tb^{3+}), respectively; $n = 6$, 8, and 10 corresponding to dipole–dipole (d–d), dipole–quadrupole (d–q), and quadrupole–quadrupole (q–q) interactions, respectively. The $I_{S0}/I_S \sim C^{n/3}$ plots are illustrated in Fig. 8. Best linear behavior can be observed only when $n = 8$, indicating that energy transfer from Ce^{3+} to Tb^{3+} occurred via the electric dipole–quadrupole interaction (d–q) mechanism in the $Ca_9Sr(PO_4)_6Cl_2$ host.

Color chromaticity

Because the spectral components can be greatly changed with the increase of Tb^{3+} concentration, as a result, the PL emitting colors can be tuned. In order to more intuitionistically observe the effect of Ce^{3+} doping concentration on PL emission colors, the Commission International del'Eclairage (CIE) chromaticity coordinates of $Ca_9Sr(PO_4)_6Cl_2$:5%Ce^{3+}, y%Tb^{3+} ($0 \leq y \leq 7$) phosphors were calculated and the typical results are shown in Table 1 and Fig. 9. It can be seen that the chromaticity coordinates tune from (0.169, 0.151) to (0.258, 0.460) with increasing the concentration of Tb^{3+} from 0 to 7 %. Correspondingly, the color tone of the phosphors can be adjusted from indigo to green under the excitation of UV light, which suggests that the phosphor may have potential application for n-UV pumped WLEDs.

Thermal quenching

For the application of high-power WLEDs, thermal stability is one of the most important parameters for phosphors, because it can considerably influence the light output, color rendering index, and stability of devices. Herein, temperature-dependent emission spectra of the selected $Ca_9Sr(PO_4)_6Cl_2$:5%Ce^{3+}, 5%Tb^{3+} phosphor at different temperatures from 298 to 573 K under the excitation of 324 nm are shown in Fig. 10a. It is obvious that the emission intensities of the sample decrease with increasing temperature from 298 to 573 K. Especially, the PL intensity at 150 °C drops to be around 57.6 % of the initial value at room temperature, which suggests that the as-prepared phosphors possesses good thermal stability properties (as shown in the inset of Fig. 10a). Generally, the decrease of emission intensity is ascribed to the thermal quenching of emission intensity via phonon interaction, in which the excited luminescent center is thermally activated through the crossing point between the ground and the excited states [39, 40]. In order to calculate the activation energy (ΔE) for thermal quenching and to better understand the thermal quenching process, the temperature-dependent emission intensity is described by a modified Arrhenius equation [6, 41, 42]:

$$I_T = \frac{I_0}{1 + c\exp\left(\frac{-\Delta E}{kT}\right)}. \tag{6}$$

Herein, $I(T)$ and I_0 are the intensities of the initial and different temperatures, respectively; c is a constant; k is the Boltzmann's constant (8.617×10^{-5} eV); and ΔE is the activation energy for thermal quenching. So Eq. (6) can be rewritten as

Table 1 CIE chromaticity coordinates of $Ca_9Sr(PO_4)_6Cl_2$:5mol%Ce^{3+}, ymol%Tb^{3+} ($0 \le y \le 7$) phosphors under the excitation of 324 nm

Point no. in CIE diagram	Sample	CIE (x, y)
A	5 mol%Ce^{3+}	0.169, 0.151
B	5 mol%Ce^{3+}, 0.5 mol%Tb^{3+}	0.193, 0.241
C	5 mol%Ce^{3+}, 1 mol%Tb^{3+}	0.205, 0.281
D	5 mol%Ce^{3+}, 3 mol%Tb^{3+}	0.236, 0.385
E	5 mol%Ce^{3+}, 5 mol%Tb^{3+}	0.248, 0.427
F	5 mol%Ce^{3+}, 7 mol%Tb^{3+}	0.258, 0.460
G	5 mol %Tb^{3+}	0.267, 0.511

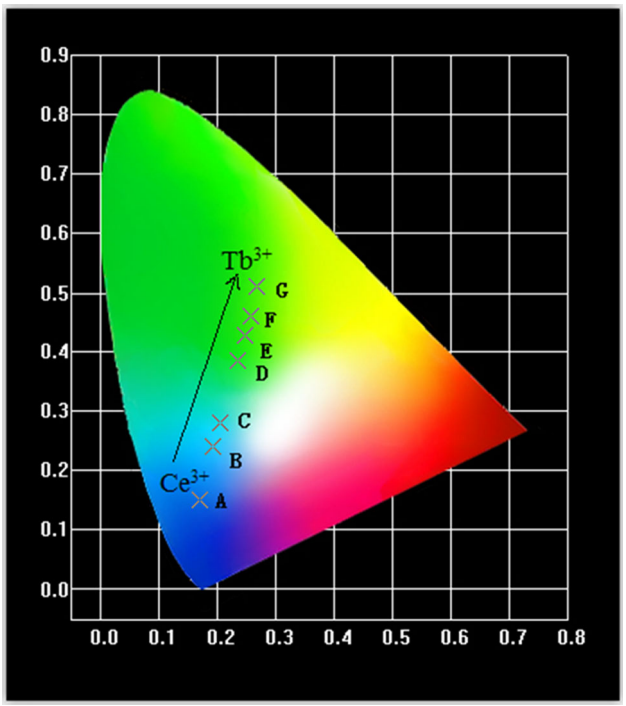

Fig. 9 CIE chromaticity diagram of $Ca_9Sr(PO_4)_6Cl_2$:5mol%Ce^{3+}, ymol%Tb^{3+} ($0 \le y \le 7$) phosphors under the excitation of 324 nm

$$\ln\left(\frac{I_0}{I}-1\right)=\ln c-\frac{\Delta E}{kT}. \quad (7)$$

According to Eq. (7), the activation energy ΔE can be calculated from a plot of $\ln[(I_0/I)-1]$ against $1/kT$. As shown in Fig. 10b, a linear fitting can be obtained using Eq. (7). The slope of the linear line equals $-\Delta E$. Thus, the ΔE was deduced to be 0.176 eV.

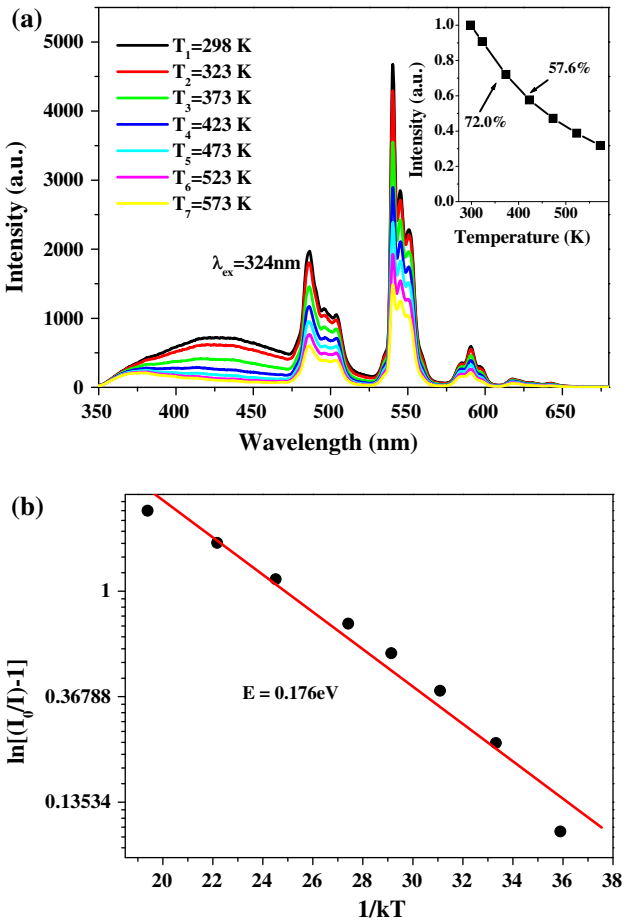

Fig. 10 **a**The PL spectra ($\lambda_{ex} = 324$ nm) of $Ca_9Sr(PO_4)_6Cl_2$:5-mol%Ce^{3+}, 5mol%Tb^{3+} phosphor at different temperatures from 298 K to 573 K. The inset shows the relative intensity as a function of temperature of the selected phosphor. **b** A fitting line of $\ln[(I_0/I)-1]$ vs.$1/kT$ activation energy graph for thermal quenching of the corresponding sample

Conclusions

To sum up, a series of Ce^{3+}-doped and Ce^{3+}/Tb^{3+} co-doped $Ca_9Sr(PO_4)_6Cl_2$ phosphors have been prepared via solid-state reaction successfully. The optimal doping concentration of Ce^{3+} ions in $Ca_9Sr(PO_4)_6Cl_2$ phosphor was confirmed to be 5 mol%. Moreover, an obvious redshift of emission band was observed with the increase of Ce^{3+}. For the Ce^{3+}/Tb^{3+} co-doped $Ca_9Sr(PO_4)_6Cl_2$ phosphor, the emission intensity of Ce^{3+} ions dramatically decreases with the increase of Tb^{3+} ion concentration because of an energy transfer from Ce^{3+} to Tb^{3+}. Moreover, the energy transfer efficiency increases greatly with the increase of Tb^{3+} ion concentration. The mechanism of energy transfer

between Ce^{3+} and Tb^{3+} was deduced to be electric dipole–dipole–quadrupole interaction. The results of temperature-dependent emission spectra indicate that the $Ca_9Sr(PO_4)_6Cl_2$: Ce^{3+},Tb^{3+} phosphor has excellent thermal stability of luminescence. The results above suggest that the as-prepared phosphors can be used as blue and green components for n-UV pumped WLEDs.

Acknowledgements This work was partially supported by the National Natural Science Foundation of China (NSFC, 51302182), the National High Technology Research and Development Program ("863" Program) of China (2015AA016901), the Qualified Personnel Foundation of Taiyuan University of Technology (QPFT) (No: tyutrc201361a), and the Program for the outstanding Innovative Teams of Higher Learning Institutions of Shanxi.

References

1. Radkov E, Bompiedi R, Srivastava AM, Setlur AA, Becker C (2004) White light with UV LEDs. Proc SPIE 5187:171–177
2. Liang C, You HP, Fu YB, He JH (2015) A novel tunable blue-green-emitting $CaGdGaAl_2O_7:Ce^{3+}$, Tb^{3+} phosphor via energy transfer for UV-excited white LEDs. Dalton Trans 44:8100–8106
3. Im WB, Brinkley S, Hu J, Mikhailovsky A, DenBaars SP, Seshadri R (2010) $Sr_{2.97-x}Ba_xCe_{0.025}AlO_4F$: a highly efficient green-emitting oxyfluoride phosphor for solid state white lighting. Chem Mater 22:2842–2849
4. Guo CF, Jing H, Li T (2012) Green-emitting phosphor $Na_2Gd_2B_2O_7:Ce^{3+}$, Tb^{3+} for near-UV LEDs. RSC Adv 2:2119–2122
5. Wu JL, Gundiah G, Cheetham AK (2007) Structure-property correlations in Ce-doped garnet phosphors for use in solid state lighting. J Chem Phys Lett 441:250–254
6. Lee GY, Han JY, Im WB, Cheong SH, Jeon DY (2012) Novel blue-emitting $Na_xCa_{1-x}Al_{2-x}Si_{2+x}O_8:Eu^{2+}$ ($x = 0.34$) phosphor with high luminescent efficiency for UV-pumped light-emitting diodes. Inorg Chem 51:10688–10694
7. Lin HC, Yang CY, Das S, Chung-Hsin Lu (2014) Photoluminescence properties of color-tunable $Ca_3La_6(SiO_4)_6:Ce^{3+}$, Tb^{3+} phosphors. J Am Ceram Soc 97:1866–1872
8. Duan CJ, Zhang ZJ, Rosler S, Delsing A, Zhao JT, Hintzen HT (2011) Preparation, characterization, and photoluminescence properties of Tb^{3+}, Ce^{3+}, and Ce^{3+}/Tb^{3+}-activated $RE_2Si_4N_6C$ (RE = Lu, Y, and Gd) phosphors. Chem Mater 23:1851–1861
9. Cao CY, Yang HK, Chung JW, Moon BK, Choi BC, Jeong JH, Kim KH (2011) Hydrothermal synthesis and enhanced photoluminescence of Tb^{3+} in Ce^{3+}/Tb^{3+} doped $KGdF_4$ nanocrystals. J Mater Chem 21:10342–10347
10. Maggay IVB, Lin PC, Liu WR (2015) Investigation of luminescence properties and the energy transfer mechanism of $Li_6Lu(BO_3)_3:Ce^{3+}$, Tb^{3+} green-emitting phosphors. RSC Adv 5:5591–5597
11. Xia ZG, Wu WW (2013) Preparation and luminescence properties of Ce^{3+} and Ce^{3+}/Tb^{3+}-activated $Y_4Si_2O_7N_2$ phosphors. Dalton Trans 42:12989–12997
12. Nohara A, Takeshita S, Isobe T (2014) Mixed-solvent strategy for solvothermal synthesis of well-dispersed $YBO_3:Ce^{3+}$, Tb^{3+} nanocrystals. RSC Adv 4:11219–11224
13. Chen MY, Xia ZG, Liu QL (2015) Luminescence properties and energy transfer of Ce^{3+}/Tb^{3+} co-doped $Ca_6Ba(PO_4)_4O$ phosphor for near-UV pumped light-emitting diodes. J Mater Chem C 3:4197–4204
14. Park WB, Singh SP, Pyo M, Sohn KS (2011) $Y_{6+x/3}Si_{11-y}Al_yN_{20+x-y}O_{1-x+y}:Re^{3+}$ (Re = Ce^{3+}, Tb^{3+}, Sm^{3+}) phosphors identified by solid-state combinatorial chemistry. J Mater Chem 21:5780–5785
15. Sayed FN, Grover V, Godboleb SV, Tyagi AK (2012) Color tunable $YF_3:Ce^{3+}/Ln^{3+}$ (Ln^{3+}: Eu^{3+}, Tb^{3+}, Dy^{3+}, Sm^{3+}) luminescent system: role of sensitizer and energy transfer study. RSC Adv 2:1161–1167
16. Jia D, Meltzer RS, Yen WM, Jia W, Wang X (2002) Green phosphorescence of $CaAl_2O_4:Tb^{3+}$, Ce^{3+} though persistence energy transfer. Appl Phys Lett 80:1535–1537
17. Zhou XF, Zhang ZY, Wang YH (2015) Ce^{3+} and Tb^{3+} singly- and co-doped $MgGd_4Si_3O_{13}$ for ultraviolet light emitting diodes and field emission displays. J Mater Chem C 3:3676–3683
18. Shmulovich J, Berkstresser GW, Brasen D (1985) Tb^{3+}-Ce^{3+} energy transfer in Tb^{3+}/Ce^{3+}: YAG single crystals. J Chem Phys 82:3078–3082
19. Blesse G, Bril A (1967) Study of energy transfer from Sb^{3+}, Bi^{3+}, Ce^{3+} to Sm^{3+}, Eu^{3+}, Tb^{3+}, Dy^{3+}. J Chem Phys 47:1920–1926
20. Sahu NK, Singh NS, Pradhan L, Bahadur D (2014) Ce^{3+} sensitized $GdPO_4:Tb^{3+}$ with iron oxide nanoparticles: a potential biphasic system for cancer theranostics. Dalton Trans 43:11728–11738
21. Pazik R, Nedelec JM, Wiglusz RJ (2014) Preferential site substitution of Eu^{3+} ions in $Ca_{10}(PO_4)_6Cl_2$ nanoparticles obtained using a microwave stimulated wet chemistry technique. CrystEngComm 16:5308–5318
22. Notzold D, Wulff H, Herzo G (1995) Structural and optical properties of the system (Ca, Sr, Eu)$(PO_4)_3Cl$. Phys Stat Sol 191:21–30
23. Wang CH, Gui DY, Qin R, Yang FL, Jing XP, Tian GS, Zhu WJ (2013) Site and local structure of activator Eu^{2+} in phosphor $Ca_{10-x}(PO_4)_6Cl_2:xEu^{2+}$. J Solid State Chem 206:69–74
24. Babu R, Jena H, Govindan Kutty KV, Nagarajan K (2011) Thermodynamic functions of $Ba_{10}(PO_4)_6Cl_2$, $Sr_{10}(PO_4)_6Cl_2$ and $Ca_{10}(PO_4)_6Cl_2$. Thermochim Acta 526:78–82
25. Fu ZL, Wang XJ, Yang Y, Wu ZJ, Duana DF, Fu XH (2014) Hydrothermal synthesis, electronic structure and tunable luminescence of single-phase $Ca_5(PO_4)_3F:Tb^{3+}/Eu^{3+}$ microrods. Dalton Trans 43:2819–2827
26. Zhou L, Liang HB, Peter AT, Zhang Su, Hou DJ, Liu CM, Tao Y, Huang Y, Li LN (2013) Luminescence, cathodoluminescence and Ce^{3+}/Eu^{2+} energy transfer and emission enhancement in the $Sr_5(PO_4)_3Cl:Ce^{3+}$, Eu^{2+} phosphor. J Mater Chem C 1:7155–7165
27. Wu JL, Gundiah G, Cheetham AK (2007) Structure-property correlations in Ce-doped garnet phosphors for use in solid state lighting. Chem Phys Lett 441:250–254
28. Zhang XG, Gong ML (2014) Single-phased white-light-emitting $NaCaBO_3:Ce^{3+}$, Tb^{3+}, Mn^{2+} phosphors for LED applications. Dalton Trans 43:2465–2472
29. Wang DY, Huang CH, Wu YC, Chen TM (2011) $BaZrSi_3O_9:Eu^{2+}$: a cyan-emitting phosphor with high quantum efficiency for white light-emitting diodes. J Mater Chem 21:10818–10822
30. Blasse G (1969) Energy transfer in oxidic phosphors. Philips Res Rep 24:131–136
31. Antipeuko BM, Bataev IM, Ermolaev VL, Privalova TA (1970) Ion-to-ion radiationless transfer of electron excitation energy between rare-earth ions in $POCl_3$-$SnCl_4$. Opt Spektrosk 29:335
32. Ozawa L, Jaffe PM (1971) The mechanism of the emission color shift with activator concentration in Eu^{3+} activated phosphors. J Electrochem Soc 118:1678–1679
33. Van Uitert L (1976) Characterization of energy transfer interactions between rare earth ions. J Electrochem Soc 114:1048–1053

34. Cheng SD, Kam CH, Buddhudu S (2001) Enhancement of green emission from Tb^{3+}: GdOBr phosphors with Ce^{3+} ion co-doping. Mater Res Bull 36:1131–1137
35. Dong J, Wang L, Cui CE, Tian Y, Huang P (2015) Luminescence properties of Ce^{3+}-doped and Ce^{3+}-Tb^{3+} co-doped $Na_{0.34}Ca_{0.66}Al_{1.66}Si_{2.34}O_8$ phosphor for UV-LED. Ceram Int 41:1341–1346
36. Bourcet JC, Fong FK (1974) Quantum efficiency of diffusion limited energy transfer in $La_{1-x-y}Ce_xTb_yPO_4$. J Chem Phys 60:34–39
37. Dexter DL, Schulman JH (1954) Theory of concentration quenching in inorganic phosphors. J Chem Phys 22:1063–1070
38. Reisfeld R, Greenberg E, Velapoldi R, Barnett B (1972) Luminescence quantum efficiency of Gd and Tb in borate glasses and the mechanism of energy transfer between them. J Chem Phys 56:1698–1705
39. Hsu CH, Lu CH (2011) Structural and optical characteristics of $CeSi_3N_5$:Tb^{3+} nitridosilicate phosphors. J Am Ceram Soc 94:1320–1323
40. Reisfeld R, Lieblich-Soffer N (1979) Energy transfer from UO_2^{2+} to Sm^{3+} in phosphate glass. J Solid State Chem 28:391–395
41. Blasse G, Grabmaier BC (1994) Luminescent Materials. Springer, Berlin, pp 91–107
42. Geng K, Xia ZG, Molokeev MS (2014) Crystal structure and luminescence property of a novel blue-emitting $Cs_{2x}Ca_{2x}Gd_{2(1-x)}(PO_4)_2$:$Eu^{2+}$ ($x = 0.36$) phosphor. Dalton Trans 43:14092–14098